Cellular Uptake of Densely Packed Polymer Coatings on Gold Nanoparticles

Mingtao Liang,[†] I-Chun Lin,[†] Michael R. Whittaker,[‡] Rodney F. Minchin,[§] Michael J. Monteiro,[‡,*] and Istvan Toth[†,*]

[†]School of Chemistry and Molecular Bioscience, [‡]Australian Institute for Bioengineering and Nanotechnology, and [§]School of Biomedical Science, The University of Queensland, Brisbane QLD 4072, Australia

ABSTRACT A variety of functional polymer chains prepared by RAFT were directly grafted onto 5, 10, and 20 nm gold nanoparticles (AuNPs). The polymer shell coating the AuNPs was densely packed because of the strong binding between the trithioester groups on the polymer chain-ends and gold. It was found that due to the densely packed nature of the shell the polymer chains were significantly stretched compared to their usual Gaussian coil conformation in water. This was even evident for polymer chains where ionic repulsion between neighboring chains should be significant. Therefore, with such high grafting densities the surface properties and size of the hybrid nanoparticles should be the only contributing factors in cellular uptake in epithelial Caco-2 cells. This study has provided valuable insight into the effects of charge and size of NPs for the application of NPs in the delivery of therapeutic agents across the intestine. Our results showed that the negatively charged AuNPs were taken up by the cells with greater efficiency than the neutral AuNPs, most probably due to binding with membrane proteins. The positively charged AuNPs as expected gave the greatest uptake efficiency. Interestingly, the uptake for PNIPAM-AuNPs (hydrophobic coating at 37 °C) increased from approximately 2% efficiency after a 30 min incubation to 8% after 2 h, and was much greater than the negative or neutral AuNPs. We believe that this was due to the interplay between the hydrophobic nature of the NPs and their increased size.

KEYWORDS: gold nanoparticle · "living" radical polymerization · polymer assembly on gold nanoparticles · Caco-2 cell · uptake of coated nanoparticles

Gold nanoparticles (AuNPs) have been extensively used in the development of new catalysts,[1,2] electronic or optical devices,[3,4] and biomedical applications.[5−7] Their versatility in a wide range of applications stems from their unique physical and chemical properties directly related to particle size, shape, and interparticle distance and surface properties. In the past decade, the design and preparation of polymer-functionalized AuNPs has attracted increasing interest, not only as a means to improve the stability of nanoparticles in poor solvents but also as a way of tailoring the surface properties of nanoparticles.[8,9] The "grafting from" and "grafting to" techniques represent two main approaches to produce functionalized AuNPs.[8] The "grafting to" approach uses presynthesized polymers grafted to the AuNPs through the polymer chain-end chemical functionality. McCormick and coworkers[10] were the first to graft well-defined water-soluble polymers onto AuNPs using polymers synthesized by reversible addition−fragmentation chain transfer (RAFT). The polymers were produced with controlled chain length, chemical composition, and chain end-functionality bearing a terminal dithioester groups. These terminal groups were readily converted to thiol groups (*e.g.*, in the presence of amines) as thiol groups have a strong binding affinity to gold *via* chemisorption with a strength that approaches that of a covalent bond.[11] It has also been shown that either dithioesters or trithiocarbonate end-groups on RAFT polymers can be converted to thiols to modify and stabilize premade gold nanoparticles.[12−14] Recent studies demonstrated that both dithioester and trithiocarbonate end groups can now be used directly to modify the gold surface *via* chemisorption.[15−19]

The surface coverage of polymers or oligonucleotides on AuNPs has been found to be substantially greater than for other NPs (polystyrene or silica) due to several factors, including lability of the citrate ions adsorbed on the naked AuNP surface and the high binding affinity of thiols to gold.[11] Consequently, this high surface packing leads to greater electrostatic and/or steric stabilization of the AuNPs, and thus provides an ideal NP system for the study of their surface interactions in biological systems.

Despite the huge potentials of AuNPs in biomedical applications,[20,21] there have been few systematic studies to investigate the role that size and surface properties of these nanoparticles play in determining their interactions with cells.[22,23] Chan *et al.* previously showed that the size and shape

*Address correspondence to m.monteiro@uq.edu.au, i.toth@uq.edu.au.

Received for review August 30, 2009 and accepted November 23, 2009.

Published online November 30, 2009. 10.1021/nn9011237

© 2010 American Chemical Society

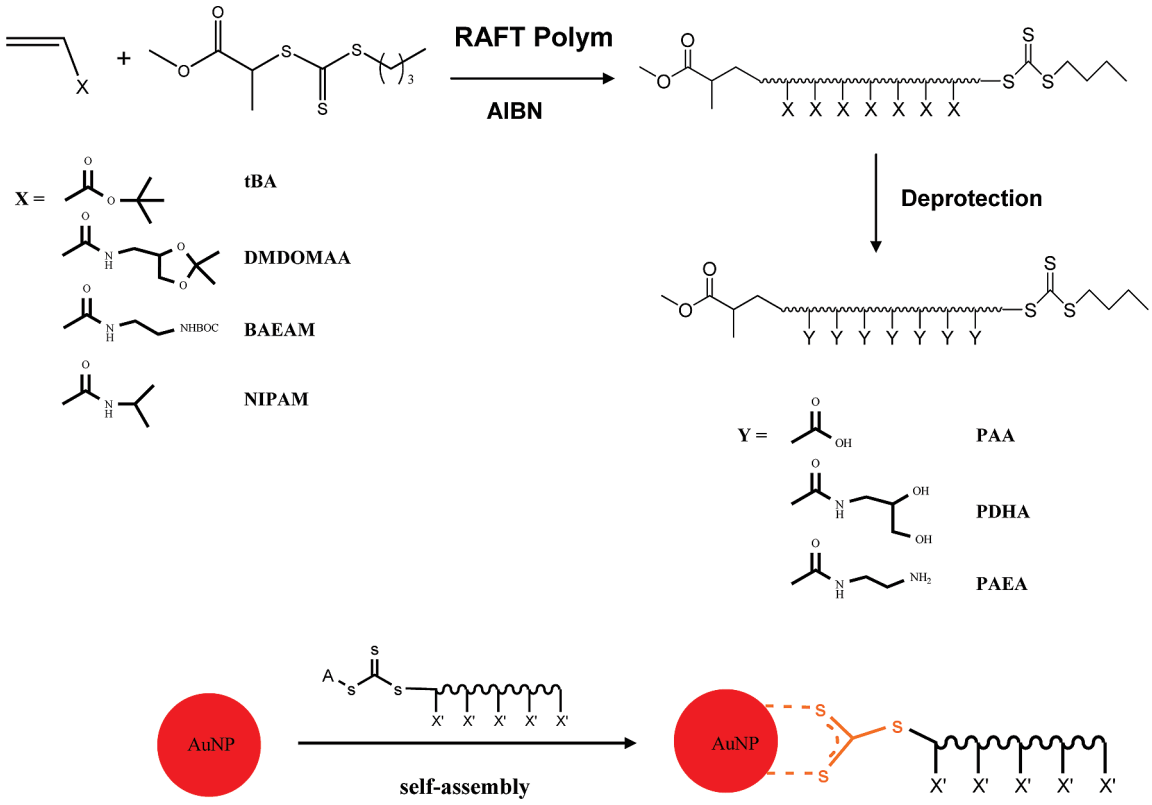

Scheme 1. Schematic of synthesis of polymers and polymer-functionalized AuNPs.

of AuNPs affects their uptake by HeLa cells.[22] In this study, 50 nm was identified as the optimum particle size for cellular uptake in comparison to both 14 and 74 nm of AuNPs. Shape was also found to play an important role during the cell uptake with fewer rod-shaped nanoparticles taken up by cells than spherical nanoparticles. Chan and other groups[24,25] found that positively charged gold nanorods exhibited higher cellular uptake than negatively charged ones, but the amount of uptake was also dependent on the chemical composition of polymer adsorbed onto the surface. To the best of our knowledge, there are no reports that systematically study the cellular uptake of spherical AuNPs with well-defined size and surface properties.

With the emerging interest of using AuNPs as carriers for the oral delivery of therapeutic agents,[26−28] this study aims to understand the relationships between the particle size and surface properties of AuNPs and their interaction with epithelial cells. Caco-2 cells are an established epithelia cell line derived from human colon adenocarcinoma cells, and has been widely used as *in vitro* model system for investigation of particle uptake into human intestines.[29] We specifically designed and synthesized a range of hydrophilic RAFT polymers with cationic, anionic, and neutral (*i.e.*, —OH) side chain groups (Scheme 1). In addition, a thermoresponsive RAFT polymer was synthesized that is hydrophilic below its lower critical solution temperature (LCST) of 32 °C and hydrophobic above this temperature. These polymers were then grafted to 5, 10, and 20 nm diameter AuNPs, and their surface properties, including surface charge, number of polymer chains per particle, packing density of the polymer chains on the surface, and footprint of a polymer chain, were investigated in relationship to uptake by Caco-2 cells.

RESULTS AND DISCUSSION

The RAFT-mediated polymerization of all monomers shown in Scheme 1 gave polymers with desired number-average molecular weight (M_n) as measured by size-exclusion chromatography (SEC).[30−32] Table 1 shows that the polydispersity indexes, PDI(SEC)s, of all polymers were low representing relatively narrow molecular weight distributions. The M_n values obtained from SEC (using a polystyrene calibration curve) were close to that found from ^{1}H NMR. The differences can be ascribed to the different hydrodynamic volume of the different polymers through the SEC columns. We be-

TABLE 1. Molecular Weight Data for the Polymers Synthesized Using the RAFT Process

RAFT polymer	M_n (SEC)[a]	PDI (SEC)[a]	M_n (NMR)[b] g/mol	degree of polymerization (n)[b]
PtBA	2940	1.10	2680	19
PDMDOMAA	3930	1.18	5060	26
PBAEAM	4910	1.13	5390	24
PNIPAM	7000	1.10	5110	43

[a] M_n values and polydispersity (PDI) were obtained from size exclusion chromatography (SEC) in THF with polystyrene calibration. [b] Degree of polymerization (n) was calculated from ^{1}H NMR spectra.

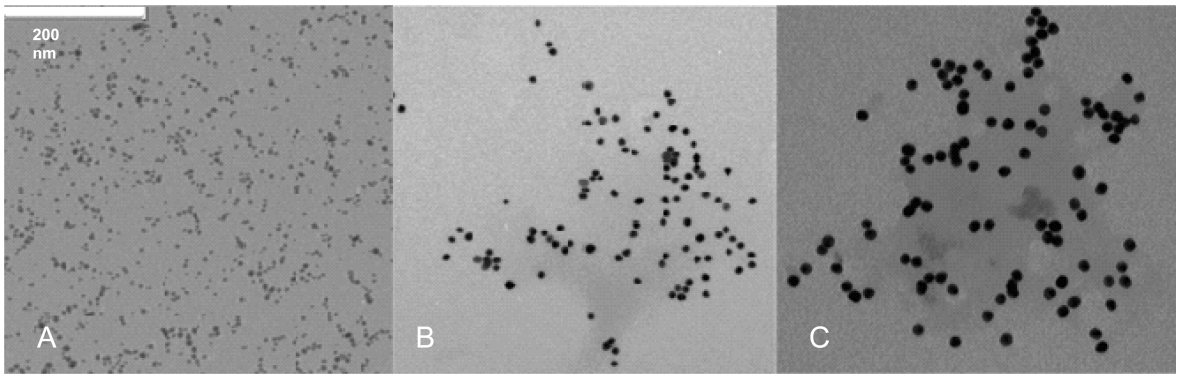

Figure 1. Representative TEM images for (A) ~5 nm, (B) ~10 nm, and (C) ~20 nm naked AuNPs prepared in present study.

lieve that the ^{1}H NMR M_n values were more accurate and were therefore used to calculate the degree of polymerization given in Table 1. The first three polymers in the series were then deprotected using TFA or HCl to give the corresponding hydrophilic polymeric species (see Scheme 1). The loss of protecting groups was confirmed by ^{1}H NMR and the formation of functional groups by FTIR (see Supporting Information). In combination, these results revealed near quantitative cleavage of the protecting groups on the side chains and generation of hydrophilic polymers with different charge and chemical composition.

A wealth of literature exists for the preparation of AuNPs with controlled size and shape using various reductants and stabilizing agents.[33,34] In our study, ~20 nm spherical AuNPs were synthesized by the most frequently applied citrate reduction method, first introduced by Turkevich *et al.*[35] and later refined by Frens.[36] For the synthesis of AuNPs with a diameter of ~10 nm, we improved on this method by adding $HAuCl_4$ solution to a boiled solution of sodium citrate under stirring.[37] Small AuNPs with a diameter of ~5 nm were prepared using $NaBH_4$ as reductant and sodium citrate as stabilizing agent.[38] Both DLS and TEM were used to determine the size and uniformity of the prepared AuNPs. Typical results of hydrodynamic diameter measured by DLS for three different size AuNPs can be found in the Supporting Information (Figure S5). These results revealed that a range of AuNPs were successfully prepared having well-defined number-average particle sizes of 18.2 ± 1.5, 11.1 ± 0.9, and 4.9 ± 0.4 nm, respectively. The polydispersity index, PDI(DLS), of the particle size distributions as measured by DLS for all the AuNPs prepared was less than 0.1, suggesting that all the particle size distributions were very narrow. This observation was further supported by TEM micrographs of typical AuNPs prepared in this study (Figure 1). In general, monodisperse spherical AuNPs were formed with aspect ratio, that is, the ratio of the long to the short axes, typically between 1.05 and 1.25. Throughout this study, the average size and particle size distribution of the AuNPs was determined for each sample TEM image from the diameter of at least 100 particles. The standard deviation of all nanoparticle sizes (5, 10, and 20 nm) was less than 10%.

It has been well-documented that sulfur-containing groups tend to exhibit a high binding affinity toward gold surfaces. Duwez *et al.* and other groups[15−18] recently demonstrated that polymers synthesized by RAFT polymerization with trithiocarbonates as the CTA can be used directly to prepare brushes on gold surface. Therefore, in the present study, the binding of RAFT polymer onto the surface of AuNPs could be achieved in one-step process simply by mixing the appropriate aqueous solution of polymer with a AuNP aqueous solution (Scheme 1). This coating process was straightforward for RAFT polymers containing carboxyl or hydroxyl functional groups. These polymers were dissolved in water and added dropwise into the citrate-stabilized AuNPs in water to prepare carboxyl functionalized AuNPs (PAA-AuNPs) or hydroxyl functionalized AuNPs (PDHA-AuNPs). However, upon the addition of a solution of amine polymers (PAEA) aggregation of AuNPs rapidly occurred, through the observation of a color change from bluish purple to dark black often leading to complete precipitation within a few minutes. The aggregation was attributed to a large excess of citrate ions remaining in the solution of AuNPs after synthesis, acting together with the oppositely charged polyamine polymer chains to induce particle flocculation.[39] For this reason, prior to being mixed with amine polymer solution, the AuNP solution was first treated with an ion-exchange resin, such as Amberlite MB-150, for 15 min to remove excessive citrate.[40] The successful removal of citrate was determined by the drop in conductivity of AuNP suspension from ~1 to ~0.02 mS/cm. This "citrate-free" AuNP solution was then added slowly into a solution of amine polymer under vigorous stirring to prepare well-dispersed amine-functionalized AuNPs (PAEA-AuNPs).

The sensitivity of the surface plasmon band of AuNPs by UV−vis spectroscopy was used to study changes in both the shape of AuNPs and any small changes to its surface. This technique is a quick but powerful tool to analyze the aggregation behavior of AuNPs and has been used extensively for analyzing par-

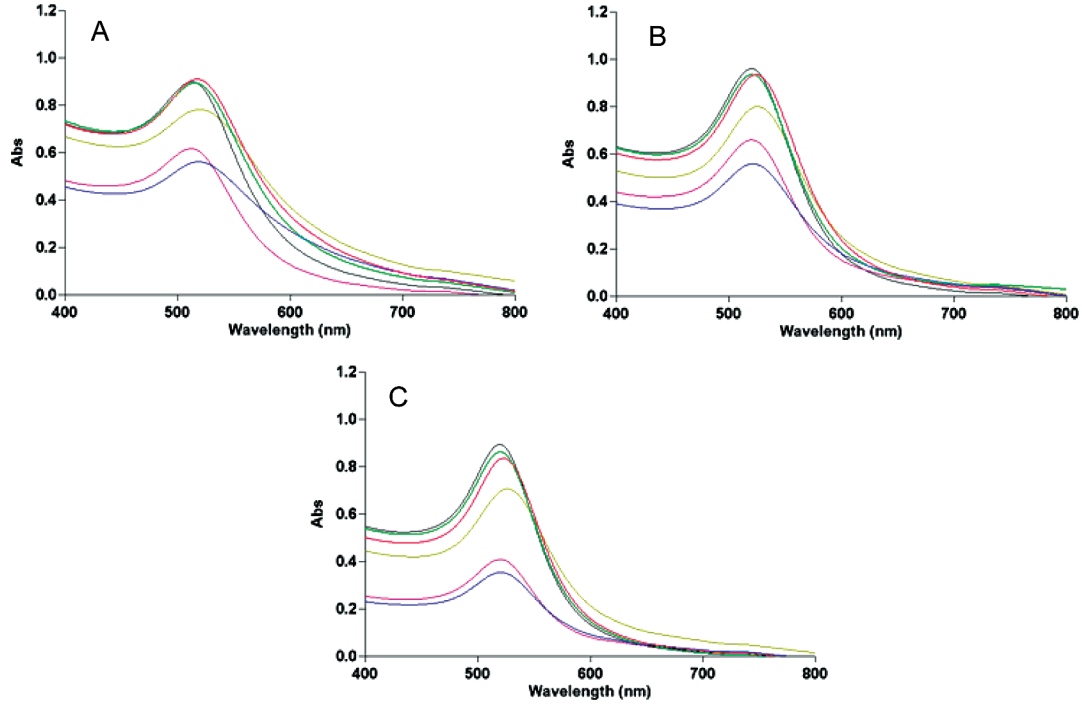

Figure 2. UV absorption spectra of "naked" AuNPs (black), citrate-free AuNPs (purple), and polymer functionalized AuNPs at a concentration of 50 μg/mL and room temperature (PAA-AuNPs, green; PDHA-AuNPs, red; PAEA-AuNPs, blue; PNIPAM-AuNPs, olive). (A) ~5 nm AuNP; (B) ~10 nm AuNP; and (C) ~20 nm AuNP.

ticle aggregation during surface functionalization in other work.[41] Figure 2 compares the UV spectra of AuNPs before and after coating with polymers. The characteristic surface plasmon band was observed at 512, 520, and 519 nm for "naked" 5, 10, and 20 nm AuNPs, respectively. After coating with carboxyl or hydroxyl polymer, the shape of the surface plasmon band was symmetrical and the bandwidth remained almost identical to that of "naked" AuNPs. This indicated that polymer-grafted AuNPs preserved the spherical shape and narrow size distribution of the original naked AuNPs with little or no particle aggregation during the coating process.[42] However, the position of plasmon band shifted slightly (~1 nm) to a longer-wavelength upon surface modification. As plasmon shifts of less than 5 nm can mainly be attributed to the change of AuNP surface environment, this minor red shift provides additional proof of surface grafting of polymer chains onto AuNPs. As shown in Figure 2, treatment of "naked" AuNPs with ion-exchange resin did not change the position or width of the surface plasmon band. In contrast, after coating AuNPs with the amine polymer, there was a noticeable increase in the bandwidth of surface plasmon band as well as a small plasmon red shift, presumably due to some particle aggregation.

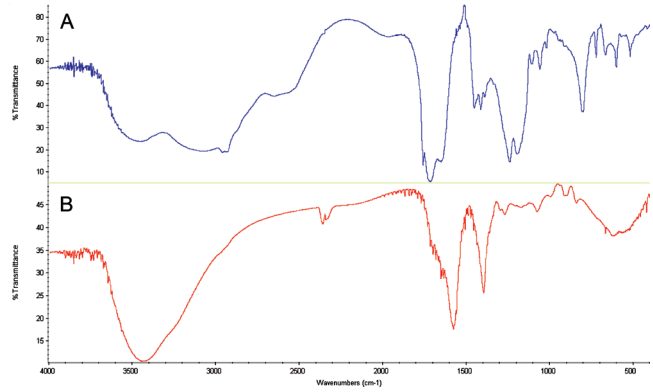

Figure 3. FTIR spectra of (A) pure PAA and (B) PAA-AuNPs.

The adsorption of polymers onto the surface of AuNPs was further investigated by mixing the solution of AuNPs with concentrated salt solution. When naked AuNPs were diluted in 1.5 M NaCl, particles, aggregation was rapid leading to visible black aggregates that precipitated out of solution. Surprisingly, relatively slower aggregation was observed for PAEA-AuNPs. This phenomenon was caused by electrostatic screening lessening the electrostatic repulsive force between PAEA-AuNPs or the competitive adsorption between chloride and amine functionalities on the surface of PAEA-AuNPs.[43] In contrast, PAA-AuNPs and PDHA-AuNPs were fairly stable in 1.5 M NaCl, as the polymer provided good steric and/or electrostatic stabilization.[44] Polymer-functionalized AuNPs were subjected to three centrifugation/washing/redispersing cycles to remove nonbound polymer, and the pellets were then collected and freeze-dried and analyzed by FTIR. Figure 3A is the representative spectrum of the RAFT synthesized PAA, which displays peaks attributed to the C═O stretching vibration at 1700 cm^{-1} and an OH stretching vibration at 3100 cm^{-1}. The spectrum of corresponding PAA-AuNPs represented in Figure 3B show the appearance

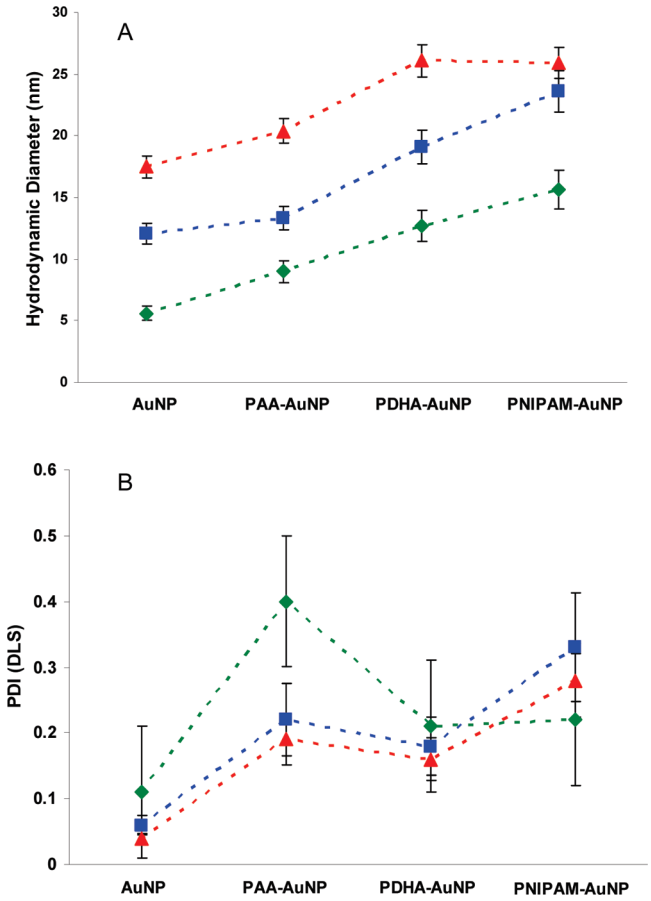

Figure 4. The effect of surface grafting of polymers on the size of AuNPs: (A) hydrodynamic diameter and (B) polydispersity index as measured by DLS (at 25 °C and a concentration of 50 μg/mL) for both naked and polymer-functionalized AuNPs (~5 nm AuNP, green; ~10 nm AuNP, blue; ~20 nm AuNP, red).

of peaks at 1700 cm^{-1} relating to the stretching vibration of the C═O bond of the carboxylic acid. The disappearance of the OH stretching vibration at 3100 cm^{-1} in Figure 3B may be attributed to a significant portion of the PAA carboxylic acid groups being in the carboxylate form, which is supported by the appearance of a peak at 1600 cm^{-1} due to the C═O stretching vibration of the carboxylate anion.[45] This provides further evidence that the AuNPs were indeed coated with the polymers. The trithiocarbonate exhibited a characteristic peak at round 1200 cm^{-1} ($\nu_{(C=S)}$) in the FTIR spectrum of PAA alone but not that of corresponding PAA-AuNPs, which suggests strong interaction of sulfur atoms with gold substrate causing loss of signal.[46] FTIR spectra also revealed the characteristic absorption signals of either OH or NH_2 groups after coating with corresponding polymers (Figure S4).

DLS measurements were performed to determine the hydrodynamic diameter of AuNPs before and after grafting with the polymers. The results revealed an increase in particle size for PAA-AuNPs, PDHA-AuNPs, and PNIPAM-AuNPs when compared with naked AuNPs (Figure 4A). In general, the particle size increase directly correlated with the increase in the molecular weight of polymer used to coat the AuNPs, with PNIPAM and hydroxyl polymer slightly larger than carboxyl polymer. This agrees with the increased light scattering upon adsorption of larger molecules on a particle surface.[47] Although the PDI(DLS) of the nanoparticle size distributions was found to increase considerably upon surface grafting (Figure 4B), analysis of TEM images revealed that polymer grafted AuNPs preserved their spherical shape with no significant particle aggregation during the grafting process. This was illustrated in Figure 5 panels A and B which show the typical TEM images of 10 nm AuNPs upon surface modification with carboxyl and hydroxyl polymers, respectively. The size and PDI(DLS) of the particle size distribution of AuNPs upon surface grafting with the amine polymer varied slightly from batch to batch. This indicated that some particle aggregation occurred during the grafting process, which was indeed confirmed by TEM image analysis. For example, after the 10 nm AuNPs were coated with the amine polymer, analysis of TEM images revealed the size of individual particles increased to approximately 14 nm, which included the thickness of polymer shell. Within the same batch of sample, some particles

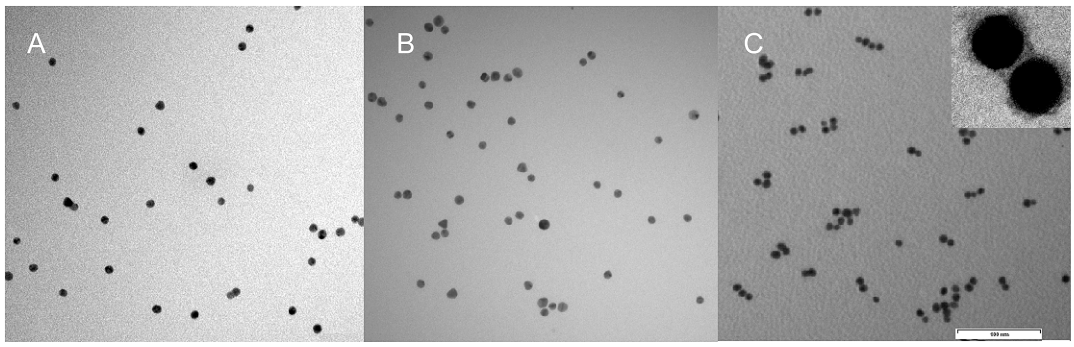

Figure 5. TEM images for ~10 nm (A) PAA-AuNPs, (B) PDHA-AuNPs, and (C) PAEA-AuNPs (scale bar = 100 nm).

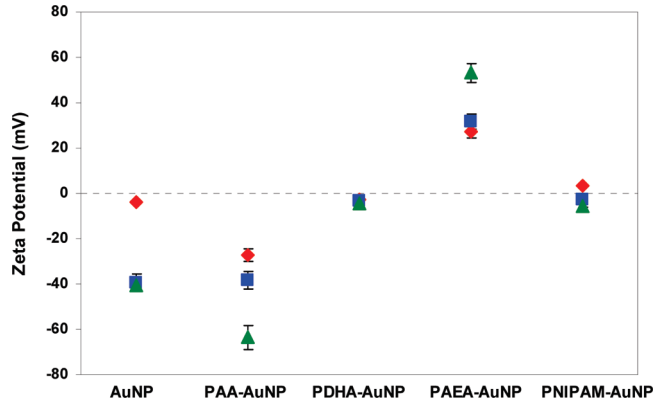

Figure 6. Zeta-potentials as measured by DLS (at 25 °C and a concentration of 50 μg/mL) for both naked and polymer-grafted AuNPs (~5 nm AuNP, red; ~10 nm AuNP, blue; ~20 nm AuNP, green).

were observed to aggregate through bridging flocculation (Figure 5C), and the aggregates were composed of double, triple, or even higher numbers of AuNPs. The surface charge (zeta potential) measurements were also carried out on AuNPs before and after grafting with polymers (Figure 6). The data clearly indicated a net negative charge for PAA-AuNPs, a neutral charge for PDHA-AuNPs and PNIPAM-AuNPs, and a net positive charge for PAEA-AuNPs.

The packing of the polymer chains on the surface of the AuNPs plays an important role in determining the surface properties of the AuNPs. In this work, we used TGA to determine the number of polymer chains bound to a particle, which allows calculations of packing density, footprint (surface area per chain), amount of polymer stretching, and the deflection angle between polymer chains[48] (see Table 2). All the polymers were found to decompose in the temperature range from 220 to 460 °C. Thus the total weight percentage of polymer grafted could be determined, and consequently the graft density of polymer chains could be calculated as follows:

$$\text{surface density of polymer (chains/nm}^2) = \frac{\left(\frac{W_{\text{polymer}}}{100 - W_{\text{polymer}}}\right)\rho V_{\text{particle}} N_A}{M_{\text{polymer}} S_{\text{particle}}} \quad (1)$$

where, W_{polymer} is the percent weight loss corresponding to the decomposition of polymer, ρ is the density of gold (19.32 g/cm^3), V_{particle} is the volume of gold nanoparticle calculated from the radius measured by TEM, N_A is Avogadro's number, M_{polymer} is the molecular weight of polymer, and S_{particle} is the surface area of gold nanoparticle.

The number of chains of PAA on the AuNP surface increased with AuNP core size. The packing density (chains/nm^2) remained relatively constant at ~1 over the AuNP size range studied at 0.1 M $NaHCO_3$, but was much greater than found for oligonucleotides (0.1−0.2 chain/nm^2 for a similar size range) at high salt concentrations (1 M NaCl) in water. Our highly packed PAA shell has a similar density to the charge neutral PNIPAM[12] or PEO[49] of 0.9 and 1.15 chains/nm^2, respectively. One would expect that even though there is some screening of the charge on the carboxylic groups on PAA, repulsion of the chains would give a surface density close to that found for the oligonucleotides. The data suggests a change in chain conformation.

The conformation of the polymer chains can be examined by the relative amount of chain stretching from its typical Gaussian conformation.[50] The dimensionless parameter, σ, can be used to describe the relative chain density on the surface and is given by the following relationship:

$$\sigma = \frac{a^2}{A_c} \quad (2)$$

where a is the length of a styrene unit (~0.25 nm) and A_c is the average surface area per corona chain. When

TABLE 2. Surface Property Data for the Grafting of Polymer Chains onto AuNPs in Water as Analyzed by TEM and TGA

	monomer units (N_A)	AuNP core diameter (nm)	density (chains/nm^2)	chains per NP	footprint (nm^2/chain)	σ	$\sigma N_A^{6/5}$	deflection angle
PAA-AuNP	19	5.4	0.95	87	1.05	0.059	2.0	24.6
		12.4	1.4	676	0.71	0.087	3.0	8.8
		18.7	1.22	1341	0.82	0.076	2.6	6.3
PDHA-AuNP	26	5.7	0.92	95	1.07	0.058	2.9	23.5
		11.9	0.97	431	1.03	0.061	3.0	11.1
		19.9	0.7	874	1.42	0.044	2.2	7.8
PAEA-AuNP	24	5.3	0.19	16	5.52	0.011	0.5	57.3
		11	0.67	281	1.35	0.046	2.1	13.7
		17.6	0.49	471	2.07	0.030	1.4	10.6
PNIPAM-AuNP	43	5.2	0.83	69	1.23	0.051	4.6	27.6
		12.2	1.04	485	0.96	0.065	5.9	10.4
		17.3	0.75	703	1.34	0.047	4.7	8.7

corona polymer chains take on a coil conformation (in a good solvent) resulting in a low surface density, each chain can be approximated to the radius of gyration. A relationship can therefore be obtained in which

$$\sigma N_A^{6/5} < 1 \quad (3)$$

Where N_A is the degree of polymerization of the corona polymer. Should $\sigma N_A^{6/5}$ be greater than 1 then the polymer chain arms are stretched, deviating in conformation from a typical Gaussian coil. The data in Table 2 shows that $\sigma N_A^{6/5}$ for PAA chains ranged from 2 to 3 representing a 2- to 3-fold increased stretching from a Gaussian coil conformation. This suggests that for the PAA chains to pack this closely in a densely brush structure there must be some ordering of the side carboxylic side groups through possible hydrogen bonding with each other or water. Obviously, if this were the case similar results should be observed for the other three polymers. The deflection angle (see eq 4)[48a] also provides information about packing. Even though the density or footprint for PAA was similar over the size range, the deflection angle for the 5.4 nm AuNP was 24.6° suggesting that PAA chains have less interaction than for the larger sizes in which the angle decreased to 8.8° for 12.4 nm and further to 6.3° for 18.7 nm.

$$\text{deflection (deg)} = \frac{2\left(\frac{\text{footprint}}{\pi}\right)^{0.5}}{r_{\text{AuNP}}}\frac{180}{\pi} \quad (4)$$

With the exception of PAEA-AuNP, both PDHA-AuNPs and PNIPAM-AuNPs gave similar results, suggesting that grafting of neutrally charged polymers onto Au produced highly packed and dense polymer shells. The only real difference between the PAA, PDHA, and PNIPAM grafting was the extraordinary stretching of the PNIPAM chains, which was approximately 4.5−6 times greater than their Gaussian coil size. In the case of the cationic PAEA-AuNPs, polymers were much less densely packed, less stretched, and with a greater deflection angle. The reason for this difference could be the interaction between the positively charged polymer and the negatively charged naked AuNP, leading to multiple binding sites of the amines from the same polymer chain onto the surface.[51] Another and probably more significant contribution is the high binding constant of amine groups to Au (N−Au bond: 6 kcal/mol),[52] also leading to a partial wrapping around the AuNP and thus reducing the number of chains that bound to the surface. This was clearly exemplified for the 5.3 nm PAEA-AuNP (see Figure S6). However, at sizes of 11 and 17 nm, PAEA chains form brushes on the gold surface, suggesting that the trithiocarbonate groups on the polymer chain ends bind rapidly and strongly to the gold surface thereby restricting the binding of other groups to the surface.

A number of studies have reported that the size of AuNPs played an important role in their cellular uptake.[22,53,54] In our study, we investigated the Caco-2 cell uptake of AuNPs by applying different concentration of nanoparticles and incubation times. As AuNPs were coated with densely packed polymers, the size and surface properties of AuNPs are the sole contributors to their interactions with Caco-2 cells. Figure 7 shows, in the range of studied particle size (~5 to 20 nm), cellular uptake of AuNPs was significantly affected by the surface charge of particles but not the size. In general, the uptake efficiency of the positively charged PAEA-AuNPs was 4−30 times greater than that of the neutral PDHA-AuNPs and negatively charged PAA-AuNPs. The neutral PDHA-AuNPs showed the lowest level of uptake over the incubation periods. The high uptake of positively charged nanoparticles could be explained by the fact that the cell membrane itself is negatively charged, therefore, positively charged nanoparticles should adhere to cell membranes and facilitate the penetration into cells.[55] Interestingly, the negatively charged PAA-AuNPs were taken up by cells at a relatively higher level than neutral PDHA-AuNPs. After incubation, cells with small AuNPs (~5 nm) at a concentration of 50 μg/mL for 2 h, the uptake efficiency of negatively charged PAA-AuNPs was almost close to 5% in comparison to less than 1% for neutral PDHA-AuNPs. Interactions with some surface molecules on cell membranes may be responsible for the facilitated uptake of negatively charged nanoparticles.[56,57] Our results further indicated that the uptake of polymer-functionalized AuNPs by Caco-2 cells was dependent on the concentration of nanoparticles in cell culture medium as well as incubation time. This result is consistent with previous observations for characterization of nanoparticle uptake by endothelial cells.[58]

In our study, a thermo-responsive neutral polymer PNIPAM[59] was also grafted onto the surface of AuNPs as a comparison to the neutral hydroxyl polymers. As measured by DLS, the PNIPAM-AuNPs had a neutral surface charge (~0 ± 5 mV) and similar sizes as those of neutral PDHA-AuNPs. However, the cell uptake efficiency of PNIPAM-AuNPs at 37 °C was much higher than that noted for PDHA-AuNPs. At this incubation temperature or temperatures above the lower critical solution temperature (LCST ≈ 32 °C[60]) of PNIPAM in water, PNIPAM collapses from a coil to globule conformation and becomes hydrophobic.[61] The size and charge of PNIPAM-AuNPs at this temperature were analyzed by DLS (Table 3). The size increased from approximately 15 to 110 nm and the zeta potential decreased from approximately zero to −3.4 mV for the ~5 nm AuNPs. For the ~10 and ~20 nm AuNPs, the size increased substantially to between 570 and 590 nm, and the zeta potential decreased to approximately −20 mV. It should be noted that the same concentration of PNIPAM-AuNPs used in the Caco-2 cell studies was analyzed by

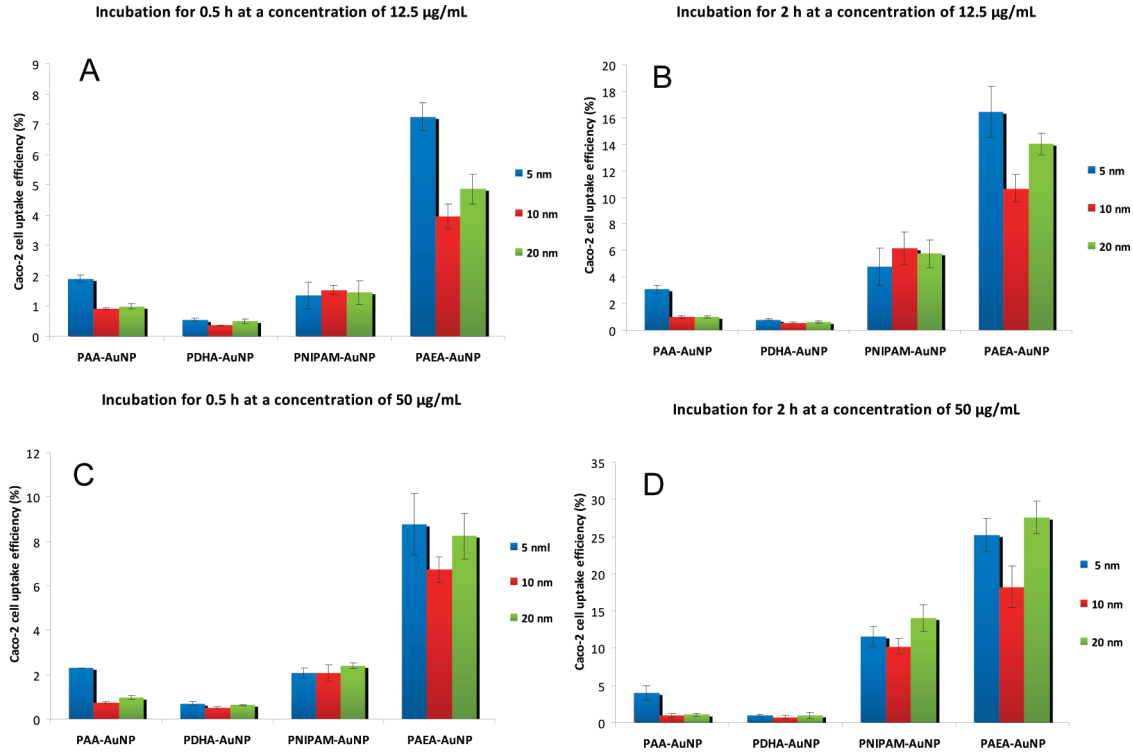

Figure 7. Cellular uptake efficiency of surface-modified AuNPs by Caco-2 cells (small, ~5 nm AuNP; medium, ~10 nm AuNP; large, ~20 nm AuNP).

DLS. These results suggest that above the LCST the loss of steric stabilization of the AuNPs results in large aggregates. The enhanced cell uptake of PNIPAM-AuNPs is mainly due to their hydrophobic interactions with the cell membrane and thus facilitating their uptake in the cells. However, the role of the large size PNIPAM particles cannot be discounted.[23,62]

CONCLUSION

Grafting of functional polymer made by RAFT onto AuNPs led to a densely packed polymer shell. This resulted in significant stretching of the polymer chains from their Gaussian coil conformation and reduced the effect of ionic repulsion from neighboring polymer chains. The methodology used in this work allowed nanoparticles to be synthesized with controlled size and with the densely packed polymer shell, allowing controlled surface properties. Uptake of these polymer/Au hybrid nanoparticles in Caco-2 cells was studied and showed that the negatively charged AuNPs were taken up by the cells with greater efficiency than the neutral AuNPs, most probably due to binding with membrane proteins. The positively charged AuNPs as expected gave the greatest uptake efficiency. Interestingly, the uptake for PNIPAM-AuNPs (hydrophobic coating at 37 °C) increased from approximately 2% after 30 min efficiency to close to 8% after 2 h, and was much greater than the negative or neutral AuNPs. We believe that this was due to an interplay between their hydrophobic interactions with the cell membrane and increased size. This study has provided valuable insight into the effects of charge and size of NPs for the application of NPs in the delivery of therapeutic agents across the intestine.

TABLE 3. Size and Surface Charge Characteristics of PNIPAM-AuNP at a Concentration of 50 μg/mL

	25 °C (<LCST)		37 °C (>LCST)	
	D_H (nm)	zeta potential (mV)	D_H (nm)	zeta potential (mV)
~5 nm PNIPAM-AuNP	15.8 ± 0.9	3.1 ± 0.5	110 ± 25	−3.5 ± 5.6
~10 nm PNIPAM-AuNP	23.3 ± 0.7	−2.9 ± 0.8	570 ± 45	−19.8 ± 6.0
~20 nm PNIPAM-AuNP	25.1 ± 1.3	−8.2 ± 2.5	590 ± 28	−20.8 ± 4.0

METHODS

Materials. 2,2′-Azo-bis-(isobutyronitrile) (AIBN; Fluka, 98%) was recrystallized from ethanol. Chain transfer agent (CTA) was synthesized using a modification of the method reported by Mayadunne *et al.*[63] (see Supporting Information for experimental details). Tert-butyl acrylate (^{t}BA; Aldrich, 99%) was passed through a basic alumina column to remove the inhibitor. Isopropylacrylamide (NIPAM; Aldrich, 97%) was recrystallized from a hexane/benzene mixture (10:1 v/v) and dried in a vacuum prior to use. Two of the other monomers used, ((2,2-dimethyl-1,3-dioxolane)methyl) acrylamide (DMDOMAA) and Boc-aminoethyl acrylamide (BAEAM), were synthesized using a modification of the method reported by Stahl *et al.*[64] (see Supporting Information for experimental details). Hydrogen tetrachloroaurate (III) hydrate ($HAuCl_4 \cdot 3H_2O$; Aldrich, 99.9%),

sodium borohydrate ($NaBH_4$; Aldrich, 98%), trisodium citrate dehydrate (Na_3Ct; Aldrich, 99%), and other chemicals were used as received. All the solvents of the highest grade were used as received. Deionized water used for experiments was purified by Milli-Q system (Millipore, Billerica, MA) with a resistance of 18.2 MΩ cm^{-1}.

The synthesis of polymers and AuNPs and the grafting of polymer onto AuNPs is given in the Supporting Information.

Analysis and Characterization Methods. ***^{1}H Nuclear Magnetic Resonance (^{1}H NMR).*** ^{1}H NMR spectra were recorded on a Bruker 300 MHz spectrometer in deuterated chloroform or water with tetramethylsilane as internal reference.

Ultraviolet—Visible Absorption (UV—vis) and Fourier Transform Infrared Spectroscopy (FTIR). UV−vis absorption spectra were recorded using a Cary 500 Scan UV−vis/NIR spectrophotometer at ambient temperature using a 1 cm quartz cell and D.I. H_2O as a standard for background correction. FTIR spectra were recorded using a Nicolet 6700 FTIR spectrometer and KBr as a standard for background correction.

Size-Exclusion Chromatography (SEC). The molecular weight distributions of polymer were measured by SEC. The dried polymer was dissolved in THF to a concentration of 1 mg/mL. This solution was then filtered through a 0.45 μm PTFE syringe filter. Analysis of the molecular weight distributions of the polymer was accomplished by using a Waters 2695 Separations Module, fitted with two Ultrastyragel linear columns (7.8 × 300 mm^2) kept in series. These columns were held at a constant temperature of 35 °C for all analyses. The columns can separate polymers in the molecular weight range of 500−2 million g/mol with high resolution. THF was used as the eluent at a flow rate of 1.0 mL/min. Calibration was carried out using narrow molecular weight PSTY standards (PDI(SEC) < 1.1) ranging from 500 to 2 million g/mol. Data acquisition was performed using Waters Millenium software (version 3.05.01) and molecular weights were calculated by using a fifth order polynomial calibration curve.

Dynamic Light Scattering (DLS). The size and zeta potential of particles was measured by DLS which was performed using a Malvern Zetasizer Nano Series running DTS software and operating a 4 mW He−Ne laser at 633 nm. Analysis was performed at an angle of 90° and a constant temperature of 25 °C. The number-average hydrodynamic particle size and PDI(DLS) are reported. The PDI(DLS) was used to describe the width of the particle size distribution, and calculated from a Cumulants analysis of the DLS measured intensity autocorrelation function and is related to the standard deviation of the hypothetical Gaussian distribution (*i.e.*, PDI(DLS) = σ^2/Z_D^2, where σ is the standard deviation and Z_D is the Z average mean size).

Thermogravimetric Analysis (TGA). TGA was carried out using a Mettler Toledo STAR^e instrument. Samples were heated to 80 °C under an argon atmosphere and held for 30 min to remove residual solvent. Samples were then heated to 800 °C at a rate of 10 °C/min. The surface density of polymer (chains/nm^2) can be estimated by TGA according to eq 1.

Transmission Electron Microscopy (TEM). A drop of the nanoparticle solution was allowed to air-dry onto a Formvar-carbon-coated 200 mesh copper grid, and the sample was stained with 2% of phosphotungstic acid for 2 min. TEM images were then acquired on a JEOL-1010 microscope operating at an accelerating voltage of 100 kV. Approximately 200 particles were counted and measured for size distribution using AnalySIS software (Soft Imaging Systems, Megaview III, Munster, Germany).

ICP-MS Instrumentation. Gold measurements were performed using a Thermo Electron Corporation X-series ICP-MS with a Peltier cooled quartz impact bead spray chamber and a 0.4 mL/min borosilicate nebulizer (MicroMist, Glass Expansion). The instrument was operated with the following conditions: a forward power of 1300 W, cool gas flow of 13 L/min, auxiliary Ar flow of 0.9 L/min, a nebulizer Ar flow rate of 0.85 L/min, and sample uptake rate of ~0.5 mL/min. Isotopes monitored include ^{197}Au, ^{185}Re, and ^{209}Bi. Each sample was measured five times by the ICP-MS.

Cellular Uptake of AuNPs by Caco-2 Cells. Caco-2 cells (American Type Culture Collection, USA) were maintained in Dulbecco's modified Eagle's medium (DMEM) with 10% heat inactivated fetal bovine serum (Invitrogen, Australia), 1% nonessential amino acid solution, and grown in flasks. Upon reaching 80% confluence cells, the cells were washed with a 0.02% EDTA solution, and further washed with a 0.25% trypsin/EDTA solution for subculturing. The cells were then seeded onto 96-well plates (~8.4 × 10^4 cells/well) and allowed to grow for 20−28 days. Cells grown on 96-well plates were maintained with the same growth media as flasks, with an extra 1% of antibiotic solution (penicillin/streptomycin). These cells were incubated at 37 °C with 5% CO_2 and the medium was changed every 2 days.

After growing the cells on 96-well plates for 21 days, the culture medium was replaced by HBSS (Hanks' balanced salt solution, pH 7.4) buffer and preincubated at 37 °C for 30 min. The cell uptake of polymer-functionalized AuNPs was initiated by exchanging the transport medium with 100 μL of nanoparticle solution in HBSS and incubated at 37 °C for 30 min and 2 h, respectively. The cell uptake study for each sample was repeated four times. Experiment was terminated by removing the nanoparticle solution and washing the cell monolayer three times with PBS buffer. The cell-associated polymer-functionalized AuNPs were then prepared for ICP-MS analysis.

The cells from the uptake studies were lysed for 15 min using a 0.25% trypsin/EDTA solution. The resulting cell lysate was digested using aqua regia and reacted overnight. After digestion using aqua regia, each sample solution was diluted to 1 mL using Milli-Q water, and solutions of ^{185}Re and ^{209}Bi were added as internal standards. The final sample solution (3 mL) contained ~3% aqua regia and 5 ppm of ^{185}Re and ^{209}Bi. Gold standard solution (300, 150, 30, 15, 3, 0.3, 0.15, and 0.05 ppb) were prepared and used to generate a calibration line for determining the amount of gold ions present in each sample.

Acknowledgment. The authors wish to thank the Australian Research Council for funding (DP878733).

Note added after ASAP publication: In the discussion of Figures 2 and 3 in the version published November 30, 2009, the description of the plasmon shift was mis-stated. The correct version was reposted December 4, 2009.

Supporting Information Available: Synthesis of polymer and polymer-functionalized AuNPs, ^{1}H NMR, FTIR, and DLS spectra are given. This material is available free of charge *via* the Internet at http://pubs.acs.org.

REFERENCES AND NOTES

1. Corma, A.; Garcia, H. Supported Gold Nanoparticles as Catalysts for Organic Reactions. *Chem. Soc. Rev.* **2008**, *37*, 2096–2126.
2. Ishida, T.; Haruta, M. Gold Catalysts: Towards Sustainable Chemistry. *Angew. Chem., Int. Ed.* **2007**, *46*, 7154–7156.
3. Wilson, R. The Use of Gold Nanoparticles in Diagnostics and Detection. *Chem. Soc. Rev.* **2008**, *37*, 2028–2045.
4. Pingarrón, J. M.; Yáñez-Sedeño, P.; González-Cortés, A. Gold Nanoparticle-Based Electrochemical Biosensors. *Electrochim. Acta* **2008**, *53*, 5848–5866.
5. Murphy, C. J.; Gole, A. M.; Stone, J. W.; Sisco, P. N.; Alkilany, A. M.; Goldsmith, E. C.; Baxter, S. C. Gold Nanoparticles in Biology: Beyond Toxicity to Cellular Imaging. *Acc. Chem. Res.* **2008**, *41*, 1721–1730.
6. Boisselier, E.; Astruc, D. Gold Nanoparticles in Nanomedicine: Preparations, Imaging, Diagnostics, Therapies, and Toxicity. *Chem. Soc. Rev.* **2009**, *38*, 1759–1782.
7. Radwan, S. H.; Azzazy, H. M. E. Gold Nanoparticles for Molecular Diagnostics. *Expert Rev. Mol. Diagn.* **2009**, *9*, 511–524.
8. Shan, J.; Tenhu, H. Recent Advances in Polymer Protected Gold Nanoparticles: Synthesis, Properties and Applications. *Chem. Commun.* **2007**, 4580–4598.
9. Li, D.; He, Q.; Li, J. Smart Core/Shell Nanocomposites: Intelligent Polymers Modified Gold Nanoparticles. *Adv. Colloid Interface Sci.* **2009**, *149*, 28–38.
10. Lowe, A. B.; Sumerlin, B. S.; Donovan, M. S.; McCormick, C. L. Facile Preparation of Transition Metal Nanoparticles Stabilized by Well-Defined (Co)polymers Synthesized *via* Aqueous Reversible Addition-Fragmentation Chain

Transfer Polymerization. *J. Am. Chem. Soc.* **2002**, *124*, 11562–11563.
11. Templeton, A. C.; Wuelfing, W. P.; Murray, R. W. Monolayer-Protected Cluster Molecules. *Acc. Chem. Res.* **1999**, *33*, 27–36.
12. Yusa, S.-I.; Fukuda, K.; Yamamoto, T.; Iwasaki, Y.; Watanabe, A.; Akiyoshi, K.; Morishima, Y. Salt Effect on the Heat-Induced Association Behavior of Gold Nanoparticles Coated with Poly(*N*-isopropylacrylamide) Prepared *via* Reversible Addition-Fragmentation Chain Transfer (RAFT) Radical Polymerization. *Langmuir* **2007**, *23*, 12842–12848.
13. Toyoshima, M.; Miura, Y. Preparation of Glycopolymer-Substituted Gold Nanoparticles and Their Molecular Recognition. *J. Polym. Sci., Part A* **2009**, *47*, 1412–1421.
14. Aqil, A.; Qiu, H.; Greisch, J.-F.; Jérôme, R.; De Pauw, E.; Jérôme, C. Coating of Gold Nanoparticles by Thermosensitive Poly(*N*-isopropylacrylamide) End-Capped by Biotin. *Polymer* **2008**, *49*, 1145–1153.
15. Fustin, C.-A.; Colard, C.; Filali, M.; Guillet, P.; Duwez A.-S.; Meier, M. A. R.; Schubert, U. S.; Gohy, J.-F. Tuning the Hydrophilicity of Gold Nanoparticles Templated in Star Block Copolymers. *Langmuir* **2006**, *22*, 6690–6695.
16. Duwez, A.-S.; Guillet, P.; Colard, C.; Gohy, J.-F.; Fustin, C.-A. Dithioesters and Trithiocarbonates as Anchoring Groups for the "Grafting-To" Approach. *Macromolecules* **2006**, *39*, 2729–2731.
17. Hotchkiss, J. W.; Lowe, A. B.; Boyes, S. G. Surface Modification of Gold Nanorods with Polymers Synthesized by Reversible Addition-Fragmentation Chain Transfer Polymerization. *Chem. Mater.* **2006**, *19*, 6–13.
18. Merican, Z.; Schiller, T. L.; Hawker, C. J.; Fredericks, P. M.; Blakey, I. Self-Assembly and Encoding of Polymer-Stabilized Gold Nanoparticles with Surface-Enhanced Raman Reporter Molecules. *Langmuir* **2007**, *23*, 10539–10545.
19. Boyer, C.; Whittaker, M. R.; Luzon, M.; Davis, T. P. Design and Synthesis of Dual Thermoresponsive and Antifouling Hybrid Polymer/Gold Nanoparticles. *Macromolecules* **2009**, *42*, 6917–6926.
20. Sperling, R. A.; Gil, P. R.; Zhang, F.; Zanella, M.; Parak, W. J. Biological Applications of Gold Nanoparticles. *Chem. Soc. Rev.* **2008**, *37*, 1896–1908.
21. Ghosh, P.; Han, G.; De, M.; Kim, C. K.; Rotello, V. M. Gold Nanoparticles in Delivery Applications. *Adv. Drug Delivery Rev.* **2008**, *60*, 1307–1315.
22. Chithrani, B. D.; Ghazani, A. A.; Chan, W. C. W. Determining the Size and Shape Dependence of Gold Nanoparticle Uptake into Mammalian Cells. *Nano Lett.* **2006**, *6*, 662–668.
23. Salmaso, S.; Caliceti, P.; Amendola, V.; Meneghetti, M.; Magnusson, J. P.; Pasparakis, G.; Alexander, C. Cell Up-Take Control of Gold Nanoparticles Functionalized with a Thermoresponsive Polymer. *J. Mater. Chem.* **2009**, *19*, 1608–1615.
24. Hauck, T. S.; Ghazani, A. A.; Chan, W. C. W. Assessing the Effect of Surface Chemistry on Gold Nanorod Uptake, Toxicity, and Gene Expression in Mammalian Cells. *Small* **2008**, *4*, 153–159.
25. Alkilany, A. M.; Nagaria, P. K.; Hexel, C. R.; Shaw, T. J.; Murphy, C. J.; Wyatt, M. D. Cellular Uptake and Cytotoxicity of Gold Nanorods: Molecular Origin of Cytotoxicity and Surface Effects. *Small* **2009**, *5*, 701–708.
26. Hillyer, J. F.; Albrecht, R. M. Gastrointestinal Persorption and Tissue Distribution of Differently Sized Colloidal Gold Nanoparticles. *J. Pharm. Sci.* **2001**, *90*, 1927–1936.
27. Sonavane, G.; Tomoda, K.; Sano, A.; Ohshima, H.; Terada, H.; Makino, K. *In Vitro* Permeation of Gold Nanoparticles through Rat Skin and Rat Intestine: Effect of Particle Size. *Colloids Surf., B* **2008**, *65*, 1–10.
28. Joshi, H. M.; Bhumkar, D. R.; Joshi, K.; Pokharkar, V.; Sastry, M. Gold Nanoparticles as Carriers for Efficient Transmucosal Insulin Delivery. *Langmuir* **2005**, *22*, 300–305.
29. Delie, F. Evaluation of Nano- and Microparticle Uptake by the Gastrointestinal Tract. *Adv. Drug Delivery Rev.* **1998**, *34*, 221–233.
30. Moad, G.; Rizzardo, E.; Thang, S. H. Living Radical Polymerization by the RAFT Process. *Aust. J. Chem.* **2005**, *58*, 379–410.
31. Moad, G.; Rizzardo, E.; Thang, S. H. Living Radical Polymerization by the RAFT Process: A First Update. *Aust. J. Chem.* **2006**, *59*, 669–692.
32. Moad, G.; Rizzardo, E.; Thang, S. H. Toward Living Radical Polymerization. *Acc. Chem. Res.* **2008**, *41*, 1133–1142.
33. Daniel, M.-C.; Astruc, D. Gold Nanoparticles: Assembly, Supramolecular Chemistry, Quantum-Size-Related Properties, and Applications toward Biology, Catalysis, and Nanotechnology. *Chem. Rev.* **2004**, *104*, 293–346.
34. Grzelczak, M.; Perez-Juste, J.; Mulvaney, P.; Liz-Marzan, L. M. Shape Control in Gold Nanoparticle Synthesis. *Chem. Soc. Rev.* **2008**, *37*, 1783–1791.
35. Turkevich, J.; Stevenson, P. C.; Hillier, J. A Study of the Nucleation and Growth Processes in the Synthesis of Colloidal Gold. *Discuss. Faraday Soc.* **1951**, *11*, 55–75.
36. Frens, G. Controlled Nucleation for the Regulation of the Particle Size in Monodisperse Gold Suspensions. *Nat. Phys. Sci.* **1973**, *241*, 20–22.
37. Jiang, Z. L.; Zou, M. J.; Liang, A. H. An Immunonanogold Resonance Scattering Spectral Probe for Rapid assay of Human Chorionic Gonadotrophin. *Clin. Chim. Acta* **2008**, *387*, 24–30.
38. Haiss, W.; Thanh, N. T. K.; Aveyard, J.; Fernig, D. G. Determination of Size and Concentration of Gold Nanoparticles from UV−Vis Spectra. *Anal. Chem.* **2007**, *79*, 4215–4221.
39. Schneider, G. F.; Decher, G. From "Nano-bags" to "Micro-pouches. Understanding and Tweaking Flocculation-Based Processes for the Preparation of New Nanoparticle-Composites. *Nano Lett.* **2008**, *8*, 3598–3604.
40. Sharma, J.; Chhabra, R.; Yan, H.; Liu, Y. A Facile *in Situ* Generation of Dithiocarbamate Ligands for Stable Gold Nanoparticle−Oligonucleotide Conjugates. *Chem. Commun.* **2008**, 2140–2142.
41. Schneider, G. F.; Decher, G. From Functional Core/Shell Nanoparticles Prepared *via* Layer-by-Layer Deposition to Empty Nanospheres. *Nano Lett.* **2004**, *4*, 1833–1839.
42. Schneider, G. F.; Decher, G. Functional Core/Shell Nanoparticles *via* Layer-by-Layer Assembly. Investigation of the Experimental Parameters for Controlling Particle Aggregation and for Enhancing Dispersion Stability. *Langmuir* **2008**, *24*, 1778–1789.
43. Vivek, J. P.; Burgess, I. J. Insight into Chloride Induced Aggregation of DMAP-Monolayer Protected Gold Nanoparticles Using the Thermodynamics of Ideally Polarized Electrodes. *J. Phys. Chem. C* **2008**, *112*, 2872–2880.
44. Grubbs, R. B. Roles of Polymer Ligands in Nanoparticle Stabilization. *Polym. Rev.* **2007**, *47*, 197–215.
45. Hotchkiss, J. W.; Mohr, B. G. R.; Boyes, S. G. Gold Nanorods Surface Modified with Poly(acrylic acid) as a Template for the Synthesis of Metallic Nanoparticles. *J. Nanopart. Res.*, published online on July 5, 2009, http://dx.doi.org/10.1007/s11051-009-9642-x.
46. Du, B.; Zhao, B.; Tao, P.; Yin, K.; Lei, P.; Wang, Q. Amphiphilic Multiblock Copolymer Stabilized Au Nanoparticles. *Colloids Surf., A* **2008**, *317*, 194–205.
47. Housni, A.; Ahmed, M.; Liu, S.; Narain, R. Monodisperse Protein Stabilized Gold Nanoparticles *via* a Simple Photochemical Process. *J. Phys. Chem. C* **2008**, *112*, 12282–12290.
48. Hill, H. D.; Millstone, J. E.; Banholzer, M. J.; Mirkin, C. A. The Role Radius of Curvature Plays in Thiolated Oligonucleotide Loading on Gold Nanoparticles. *ACS Nano* **2009**, *3*, 418–424.
49. Corbierre, M. K.; Cameron, N. S.; Sutton, M.; Laaziri, K.; Lennox, R. B. Gold Nanoparticle/Polymer Nanocomposites: Dispersion of Nanoparticles as a Function of Capping

Agent Molecular Weight and Grafting Density. *Langmuir* **2005**, *21*, 6063–6072.
50. Zhang, L.; Eisenberg, A. Multiple Morphologies and Characteristics of "Crew-Cut" Micelle-like Aggregates of Polystyrene-*b*-poly(acrylic acid) Diblock Copolymers in Aqueous Solutions. *J. Am. Chem. Soc.* **1996**, *118*, 3168–3181.
51. Sardar, R.; Bjorge, N. S.; Shumaker-Parry, J. S. pH-Controlled Assemblies of Polymeric Amine-Stabilized Gold Nanoparticles. *Macromolecules* **2008**, *41*, 4347–4352.
52. Di Felice, R.; Selloni, A. Adsorption Modes of Cysteine on Au(111): Thiolate, Amino-Thiolate, Disulfide. *J. Chem. Phys.* **2004**, *120*, 4906–4914.
53. Yen, H. J.; Hsu, S. H.; Tsai, C. L. Cytotoxicity and Immunological Response of Gold and Silver Nanoparticles of Different Sizes. *Small* **2009**, *5*, 1553–1561.
54. Chithrani, B. D.; Chan, W. C. W. Elucidating the Mechanism of Cellular Uptake and Removal of Protein-Coated Gold Nanoparticles of Different Sizes and Shapes. *Nano Lett.* **2007**, *7*, 1542–1550.
55. Harush-Frenkel, O.; Altschuler, Y.; Benita, S. Nanoparticle-Cell Interactions: Drug Delivery Implications. *Crit. Rev. Ther. Drug Carrier Syst.* **2008**, *25*, 485–544.
56. Ghinea, N.; Simionescu, N. Anionized and Cationized Hemeundecapeptides as Probes for Cell Surface Charge and Permeability Studies: Differentiated Labeling of Endothelial Plasmalemmal Vesicles. *J. Cell Biol.* **1985**, *100*, 606–612.
57. Mailänder, V.; Landfester, K. Interaction of Nanoparticles with Cells. *Biomacromolecules* **2009**, *10*, 2379–2400.
58. Davda, J.; Labhasetwar, V. Characterization of Nanoparticle Uptake by Endothelial Cells. *Int. J. Pharm.* **2002**, *233*, 51–59.
59. Ganachaud, F.; Monteiro, M. J.; Gilbert, R. G.; Dourges, M.-A.; Thang, S. H.; Rizzardo, E. Molecular Weight Characterization of Poly(*N*-isopropylacrylamide) Prepared by Living Free-Radical Polymerization. *Macromolecules* **2000**, *33*, 6738–6745.
60. Schild, H. G. Poly(*N*-isopropylacrylamide): Experiment, Theory, and Application. *Prog. Polym. Sci.* **1992**, *17*, 163–249.
61. Urbani, C. N.; Monteiro, M. J. Nanoreactors for Aqueous RAFT-Mediated Polymerizations. *Macromolecules* **2009**, *42*, 3884–3886.
62. Bisht, H. S.; Manickam, D. S.; You, Y.; Oupicky, D. Temperature-Controlled Properties of DNA Complexes with Poly(ethylenimine)-*graft*-poly(*N*-isopropylacrylamide). *Biomacromolecules* **2006**, *7*, 1169–1178.
63. Mayadunne, R. T. A.; Jeffery, J.; Moad, G.; Rizzardo, E. Living Free Radical Polymerization with Reversible Addition-Fragmentation Chain Transfer (RAFT Polymerization): Approaches to Star Polymers. *Macromolecules* **2003**, *36*, 1505–1513.
64. Stahl, G. L.; Walter, R.; Smith, C. W. General Procedure for the Synthesis of Mono-*N*-acylated 1,6-Diaminohexanes. *J. Org. Chem.* **1978**, *43*, 2285–2286.